



Research Article

Numerical investigation of hydrothermal performances of minichannel heat sink using porous media

Rajesh KUMAR^{1,*}, Mohammad ZUNAID¹, Radhey Shyam MISHRA¹

¹Department of Mechanical Engineering, Delhi Technological University, Delhi, 110042, India

ARTICLE INFO

Article history

Received: 19 October 2023

Revised: 02 January 2024

Accepted: 02 January 2024

Keywords:

Electronic Cooling; Heat Sink; Hydrothermal Performances; Minichannel; Nanofluids; Porous Media

ABSTRACT

In the present study, 3-D CFD simulations have been performed to examine the hydrothermal performance of a circular-shaped minichannel heat sink. The heat sink is composed of aluminum with dimensions of 40mm × 40mm × 10mm and it is designed for Reynolds numbers less than 1300. A uniform heat flux of 66 KW/m² is applied to the bottom wall of the heat sink, while other surfaces have been insulated. The finite volume approach was utilized in Ansys-Fluent to solve the system governing equations and associated boundary conditions. Magnetite-water nanofluid has been used as a coolant and examined the variations of mass flow rate and nanofluid concentration on cooling potential. A bronze porous material has been inserted throughout the channel space at various porosity levels. The performances of the heat sink have been further investigated at various channel counts by varying the hydraulic diameter in a manner that the total flow area of the channels remains constant. The results show that the number of channels and their dimensions have a substantial effect on heat transfer efficiency. This investigation reveals that using porous media is very significant relative to nanofluid at any concentration and the maximum augmentation in heat transfer by the incorporation of porous media along with nanofluid is 5.54 times. Moreover, the heat sink's practical utility is optimized through figures of merit (FOM) and heat transfer efficiency. As a result, the optimum hydrothermal performance of this present study is achieved at six channels with a lower volume flow rate, higher volume fraction of nanofluid, and a lower porosity level.

Cite this article as: Kumar R, Zunaid M, Mishra RS. Numerical investigation of hydrothermal performances of minichannel heat sink using porous media. J Ther Eng 2025;11(1):141–158.

INTRODUCTION

Research on small heat exchangers has gained significant attention in the last two decades. We are all aware that the enormous heat flux generated by the devices is the main factor in component damage. Therefore, the heat flux removal mechanism has become significantly increased to keep such

equipment's temperature below acceptable standards. A minichannel heat sink develops a novel cooling technology to remove too much heat from a very compact space. The minichannel flow offers an extremely high surface area-to-volume ratio and a robust convective heat transfer coefficient. Tuckerman and Pease [1] first proposed the concept of a microchannel heat sink (MCHS). They conducted tests

*Corresponding author.

*E-mail address: rajeshkumar_2k21phdme06@dtu.ac.in

This paper was recommended for publication in revised form by Editor-in-Chief Ahmet Selim Dalkılıç



on a rectangular-shaped microchannel made up of silicon and demonstrated that miniaturization of the heat sink could significantly lower the surface temperature. Their pioneering work started another study; many researchers compared their experimental [2, 3], numerical [4, 5], and analytical [6, 7] studies with Tuckerman and Peace. They found that reducing the characteristic diameter of the channel to a micron-scale enhanced the rate of heat transmission compared with conventionally sized devices. A wide range of channel configurations, including triangular [8], trapezoidal [9], tapered [10], converging [11], and ribbed [12], have been examined and found that the geometrical variation and its optimization have a very significant effect on the heat transfer rate. Yildizeli and Cadirci [13] investigated the hydro-thermal characteristics of a rectangular MCHS numerically and optimized its performance using a multi-objective genetic algorithm known as the elitist Non-Dominated Sorting Genetic Algorithm (NSGA-II). From the result, it was found that the optimization approach significantly improves the MCHS's hydrodynamic and thermal characteristics. During the design of the MCHS, any design point located on the Pareto optimum front is chosen based on the most dominant objective. Kose et al. [14] use CFD and NSGA-II to perform a numerical analysis of conjugate heat transfer for three distinct shapes of MCHS (rectangular, triangular, and trapezoidal) to explore geometric design variables on optimum solutions. A Pareto frontal comparison of all three variants revealed that the rectangular microchannel is the most significant geometry in terms of hydrothermal performance. The literature demonstrates that the geometrical modification and its optimization is a very adequate passive technique that significantly enhances the conjugate heat transfer of MCHS.

Nanofluids have also been used in some studies to cool the heat sink. Researchers [15–17] explore the pressure drop and heat transfer coefficient of the heat sink by the incorporation of nanofluids. The outcome indicates that increasing the Peclet number, Reynolds number and nanoparticle volume fraction improve the coefficient of heat transfer. Alawi et al. [18] found that the shape and size of nanoparticles have a significant impact on thermal conductivity and fluid viscosity. Koo et al. [19] and Chein et al. [20] show that the Cu-water nanofluid in microchannel experienced better heat transfer than conventional fluids. Some researchers investigate experimentally [21, 22] and numerically [23–26], the hydrothermal behavior of Al_2O_3 - H_2O nanofluid in the rectangular-shaped MCHS. This analysis shows that employing nanofluids in the heat sink is very efficient relative to pure water at any concentration. Additionally, it was discovered that the smaller nanoparticle's dimensions with higher concentration improved the heat transfer coefficient. Sayyed et al. [27] studied the heat transfer phenomenon of SiO_2 -water nanofluids and found that the thermal resistance of the heat sink was decreased by up to 10%. Sohel et al. [28] found that employing nanofluid rather than conventional fluid lowered the rate of thermal

entropy generation. Kumar and Sarkar [29] studied the impact of hybrid nanofluid on thermal performance and found that the hydrothermal performance of hybrid nanofluid is superior to mono-nanofluid. Goud et al. [30] show that hybrid nanofluids have greater thermal dispersion than homogeneous nanofluids. Zahan et al. [31] show that the thermophysical properties and coefficient of performance of hybrid nanofluid are more significant than mono-nanofluid. Awad et al. [32] use nano-enhanced phase-change materials (PCM) to boost energy storage capability and it was concluded that adding nanoparticles to the PCM improves thermal characteristics over PCMs alone because of the interfacial layer formed in the nano-PCM. Awad and Muayad [33] studied a NaNO_3 and nano- NaNO_3 PCM for solar energy storage and it was found that the addition of nanoparticles improved charging and discharging by 25.6% and 23.93%, respectively. This study concludes that the PCMs and nano-PCMs are used in solar energy storage, emphasizing the possible advantages of integrating nanoparticles to enhance their efficiency. Luo et al. [34] performed a numerical analysis of the serpentine tube reactor for the heat discharge (hydration) process incorporated with K_2CO_3 hydrate. They conclude that increased vapor pressure has been proven to significantly raise the output temperature, while a greater flow rate of heat transfer fluid (HTF) has improved the aggregate heat exchange performance. Younis et al. [35] investigated the thermal storage performances of nano-enhanced phase change material (NEPCM) within an annulus between an outer wavy cylinder. They conclude that melting times are shortened and heat transfer is improved by increasing nanoparticle concentration. As compared to the pristine PCM, the melting time is lowered by 23.2% at a 6% nanoparticle concentration. Jahanbakhshi et al. [36] carried out a study on the thermal management of lithium-ion batteries using a microchannel heat sink with wavy microtubes. The results show that using a heat sink lowered the surface temperature of the battery in all circumstances, whereas the battery surface has a more consistent temperature profile when counterflow is used in a microtube or microchannel. The incorporation of nanofluid in this cooling system maintains its temperature within a safe working range. The literature demonstrates that the nanofluid is a very adequate passive technique that enhances the heat transfer rate more efficiently than any conventional fluids in any scenario.

A porous channel [37] is another passive technique to improve heat transfer due to strengthening the redistribution of the flow along with modification of the radiative property of the convective medium. Koh et al. [38] observed that the wall temperature of the heat sink decreases enormously when the porous material of higher thermal conductivity is inserted inside the channel. Hunt et al. [39] compared the heat transfer rate of porous channels numerically and experimentally. They reveal that employing porous material increases the heat transmission rate by 200–400% more than a non-porous heat sink. Zehforoosh and Hossainpour

[40] Studied a convection phenomenon in a partially porous channel and found that the thermal performance of a partially porous channel is more significant than a fully porous channel. Wang et al. [41] Studied the novel design of a gradient porous heat sink (GPHS) and compared it with the homogeneous porous heat sink (HPHS) and it was found that the Nusselt numbers of GPHS configuration are larger than the HPHS. Saravanan et al. [42] examined the performance of heat sinks with porous media and found that the micro/mini channel heat sink is superior when the porous medium is placed at the center or periphery. The results reveal that the performance index of the heat sink is enhanced by 13 % in comparison to a completely porous heat sink. Bezaatpour and Goharkhah [43] Carried out a numerical study of magnetite nanofluid with porous media into the heat sinks and found that at low volume flow rates, porosities, and higher nanofluid concentrations, the performance of heat sink will be enhanced. Dai et al. [44] reveal that the hydrothermal performance of porous micro /mini channel heat sinks can be enhanced by optimizing the pore size, porosity, and locations of porous materials. Sukumar et al. [45] conclude that incorporating porous media into the thermal system is the most suitable technique for augmenting the heat transfer however the local thermal non-equilibrium (LTNE) technique is accurate for modeling nanofluid and porous media. Alhajaj et al. [46] and Sivasankaran et al. [47] examined the flow behavior of the hybrid nanofluid inside a porous channel. It was found that this approach is another choice to enhance heat transfer against pressure loss. Rashidi et al. [48] carried out a thorough investigation of the capability of porous materials for thermal management of lithium-ion batteries (LIBs). The outcome reveals that the battery surface temperature decreases at lower porosity with constant pore density whereas increases by raising the pore density due to the major influence of permeability. Kaabinejadian et al. [49] investigate the incorporation of porous media and its impact on the thermal management of prismatic lithium-ion batteries employing liquid electrolytes as a coolant. The results conclude that raising the pore size leads to lowered the maximum temperature within the battery. In comparison to the non-inclined porous region, the inclined porous region greatly reduces the temperature field's standard deviation. Hosseini et al. [50] addressed the difficulties in developing innovative materials that could improve the efficiency of energy conversion and storage systems. It was proposed that the controlled porosity of cellular-based mechanical metamaterials or multiscale architected porous materials can offer optimal energy conversion and storage potential. These qualities may boost the material's energy and power density performance as well as increase the use of that material in lithium-ion batteries, fuel cells, and solar energy systems.

From the above literature, it can be concluded that there is still an opportunity for advancement in heat dissipation from electronic devices using miniaturized channels. The microchannel flow geometry offers a large convective heat

transfer coefficient although it has proven hard to execute due to the extremely high-pressure drop required to pump the cooling fluid through the channels. A minichannel can be utilized in a heat sink to provide significant heat flow and mild pressure loss. This is why a minichannel heat sink with a circular channel has been chosen because it is easier to manufacture and more reliable for electronic cooling. Efforts have been made to enhance the heat transfer rate by inserting porous media into the channels. However, such a configuration can result in increased pumping power. We needed a porous design optimization to improve heat transmission without sacrificing pumping power. The novelty of this work is to investigate the simultaneous incorporation of nanofluid and porous media into the minichannel heat sink under various scenarios and compare the results to produce a rigorous hydrothermal performance.

A thorough investigation of the preceding work suggested that relatively few works have been performed to analyse and optimize the passive heat transfer enhancement in a hybrid manner like; the simultaneous incorporation of nanofluid and porous media inside an MCHS. The current investigations are devoted to the numerical analysis of the hydrothermal performance of circular minichannel heat sinks filled through bronze porous media and incorporated with Fe_3O_4 /water nanofluids as a coolant. The consequences of different criteria like porosity (0.75-0.9), volume flow rate (0.05046-0.20184 lpm), and nanofluid volume fraction (0.01-0.03) are explored for the heat sink. All these numerical investigations will also be done for the various channel counts (5-8) by varying the hydraulic diameter in a manner that the total flow area of the channels stands consistent. Moreover, we finally optimize the heat sink's hydrothermal performance by taking into account all investigating criteria of this study.

PROBLEM STATEMENT

The schematic diagram of a compact heat sink made of an aluminum material having length (L), width (W), of 40 mm, and height (H) of 10 mm will be evolved in Figure 1. The primary focus of this research is on the cooling of microprocessor chips in electronic devices. The silicon wafer is placed on top of the microprocessor chip to evenly spread the heat generated in the chip's hotspot. The generated heat flux of the microprocessor is conducted to the heatsink and further transported away from the device through convection. The bottom wall of the minichannel heat sink is uniformly heated at 66 KW/m², whereas the remaining surfaces are insulated. The capability of the heat sink has been studied by keeping laminar flow through the channels and performing the computational simulation at various hydraulic diameters (Fig. 2), flow rates, nanofluid volume fractions, and porosities to appraise the optimal heat sink's performance. The detailed geometrical configuration of the minichannel employed in the present study is shown in Table 1.

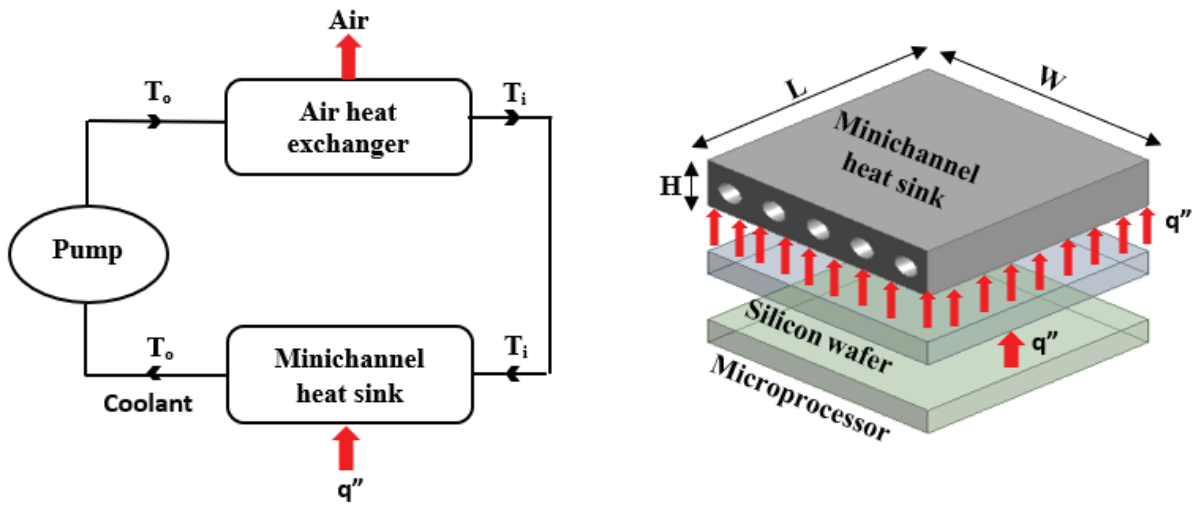


Figure 1. Schematic and working of minichannel heat sink in electronic cooling.

Table 1. Heat sink dimensions (mm)

Figure 1	L	W	H	n	Dh
a	40	40	10	5	4
b	40	40	10	6	3.6514
c	40	40	10	7	3.3806
d	40	40	10	8	3.1622

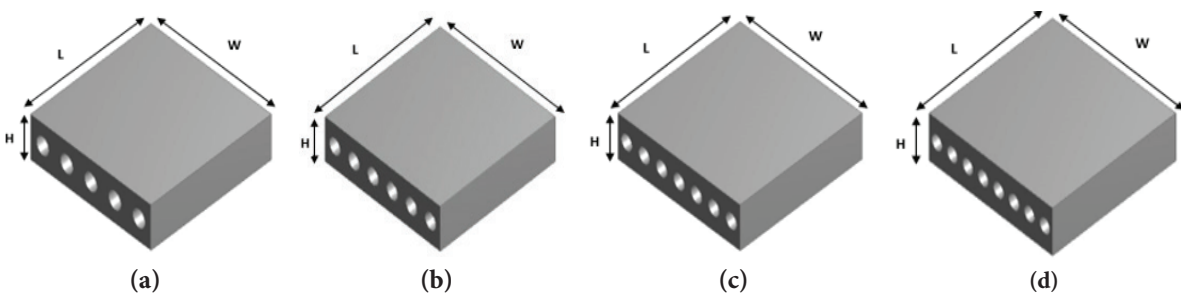


Figure 2. Heat sink schematic diagram at various channel counts (a) 5, (b) 6, (c) 7, (d) 8 respectively.

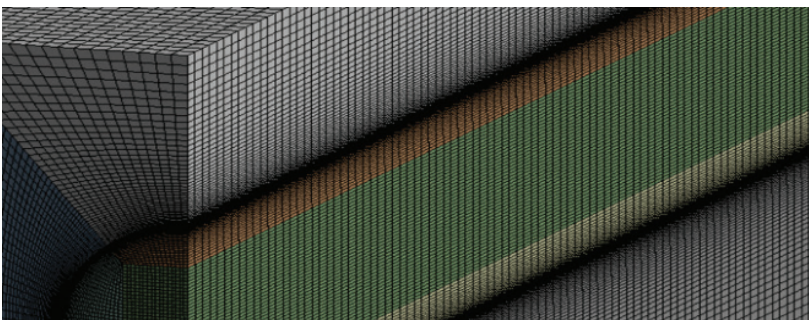


Figure 3. Represents the grid's distribution in the solid and fluid regions of the heat sinks.

Governing Equations and Boundary Conditions

Governing equations

The ensuing presumption is taken into account a) 3-D flow, b) laminar and incompressible flow, c) Steady and irrotational flow, d) Axisymmetric, e) Neglect of the body force, f) Thermal radiation is neglected, g) Thermo-physical properties is the function of temperature for nanofluid, but solid properties are taken constant, h) At interface, the fluid and solid phases are in thermal equilibrium.

Under this assumption, the following are the fluid and solid domains continuity, momentum, and energy governing equations [43].

$$\nabla \cdot (\rho_f V) = 0 \quad (1)$$

$$\frac{\rho_f}{\epsilon} \nabla \cdot \left(\frac{V \cdot V}{\epsilon} \right) = -\nabla P + \frac{\mu}{\epsilon} \nabla^2 V - \frac{\mu}{K_p} V - \frac{C_f \rho_f}{\sqrt{K_p}} |V| V \quad (2)$$

$$k_s \left(\frac{1}{r} \frac{\partial}{\partial r} \left(r \frac{\partial T_s}{\partial r} \right) + \frac{1}{r^2} \frac{\partial^2 T_s}{\partial \theta^2} + \frac{\partial^2 T_s}{\partial z^2} \right) = 0 \quad (3)$$

$$(\rho C_p)_f V \cdot \nabla T = \nabla \cdot (k_{eff} \nabla T) \quad (4)$$

Thermophysical properties of the porous domain are calculated from [43]:

$$(\rho C_p)_{eff} = (1 - \epsilon)(\rho C_p)_s + \epsilon(\rho C_p)_f \quad (5)$$

$$k_{eff} = (1 - \epsilon)k_s + \epsilon k_f \quad (6)$$

The following equation can be used to calculate the pressure drop in a channel from the inlet to the outlet.

$$\Delta P_c = \frac{128\mu QL}{\pi D^4} \quad (7)$$

The loss of energy that occurs when the fluid enters a pipe is called entry loss (ΔP_{entry}):

$$\Delta P_{entry} = k_{e1} * \frac{1}{2} \rho V_{avg}^2, (k_{e1} = 1) \quad (8)$$

The loss of energy that occurs when the fluid exits a pipe is called exit loss (ΔP_{exit}):

$$\Delta P_{exit} = k_{e2} * \frac{1}{2} \rho V_{avg}^2, (k_{e2} = 0.5) \quad (9)$$

Total pressure drops ($\Delta P = \Delta P_c + \Delta P_{entry}$)

$$\Delta P = \frac{128\mu QL}{\pi D^4} + k_{e1} * \frac{1}{2} \rho V_{avg}^2 + k_{e2} * \frac{1}{2} \rho V_{avg}^2 \quad (10)$$

The average coefficient of heat transfer is

$$h_{av} = \frac{Q}{A_h \Delta T_m} = \frac{q''}{\Delta T_m} \quad (11)$$

Where A_h denotes the convective area of heat transfer, ΔT_m is the average temperature difference between the solid wall and the fluid, and q'' represents heat flux respectively.

$$\Delta T_m = T_{ba} - T_{bu} \quad (12)$$

Here T_{ba} represents the average base temperature of the channel surface, and T_{bu} denotes the bulk mean temperature of fluid, which is defined as:

$$T_{bu} = \frac{T_{in} + T_{out}}{2} \quad (13)$$

Where T_{in} and T_{out} represent the temperature of inlet and outlet fluids correspondingly.

Thermal resistance (R_{th}) is defined as:

$$R_{th} = \frac{T_{b,max} - T_{in}}{q'' * A_h} \quad (14)$$

Here $T_{b,max}$ are the maximum bottom temperatures, respectively.

Hydraulic diameter expression for the various number of channels at constant total flow is defined as:

$$d_{fl} = \sqrt{n_i/n_{fl}} d_i \quad (15)$$

(PP) is calculated from the given formula:

$$PP = \Delta P_T * Q \quad (16)$$

wherein 'Q' represents the volume flow rate.

Heat transfer efficiency (η) is characterized by:

$$\eta = \frac{h}{h_{cf}} \quad (17)$$

Where 'cf' denotes a non-porous channel having pure water as a working fluid.

Figures of merit (FOM) is defined as:

$$FOM = \frac{h}{h_{cf}} \left(\frac{PP}{PP_{cf}} \right)^{\frac{1}{3}} \quad (18)$$

Boundary conditions

With a consistent axial velocity determined by the flow rate, the nanofluid enters the channel with a temperature of 298K at the inlet. For every analysis, the initial gauge pressure is fixed to 500 Pa, and the nanofluid exit pressure is atmospheric. The heat sink's surface is supposed to be adiabatic irrespective of the bottom surface, at which a consistent heat flux of 66 KW/m² is employed in all circumstances. Conditions for no-slip velocity and thermal equilibrium are used at solid-fluid interfaces:

$$\mathbf{u} = \mathbf{v} = \mathbf{w} = 0, (T_f)_r = (T_s)_r.$$

$$-k_{nf} \frac{\partial T_f}{\partial n} = -k_s \frac{\partial T_s}{\partial n} \quad (19)$$

Furthermore, the bottom wall condition is defined as:

$$q'' = -k_s \frac{\partial T_s}{\partial n} \quad (20)$$

And for the other wall:

$$\frac{\partial T}{\partial n} = 0 \quad (21)$$

whereas 'n' denotes the direction to surfaces normal.

Thermophysical Properties

Thermophysical properties of nanoparticles and porous media are shown in Table 2. Whereas, the following equations have been used to calculate the nanofluids properties [43].

$$(\rho)_{nf} = (1 - \varphi)\rho_f + \varphi * \rho_{np} \quad (22)$$

$$(\rho * C_p)_{nf} = (1 - \varphi)(\rho * C_p)_f + \varphi(\rho * C_p)_{np} \quad (23)$$

$$\mu_{nf} = \mu_f(1 + 2.5\varphi), \varphi \leq 2\% \quad (24)$$

$$\mu_{nf} = \frac{\mu_f}{(1 - \varphi)^{2.5}}, \varphi > 2\% \quad (25)$$

Thermal conductivity for nanofluid is evaluated by:

$$k_{nf} = k_{static} + k_{brownian} \quad (26)$$

$$k_{static} = k_f \left[\frac{((k_{np} + 2k_f) - 2\varphi(k_f - k_{np}))}{((k_{np} + 2k_f) + \varphi(k_f - k_{np}))} \right] \quad (27)$$

$$k_{brownian} = 5 * 10^4 \beta \varphi \rho_f C_{p,f} \sqrt{\frac{k_0 * T}{\rho_{nf} D_{np}}} g(\varphi, T) \quad (28)$$

Whereas, $k_0 = 1.3807 \times 10^{-23}$ J/K while 'β' is the volume proportion of liquid whose travels through the particles.

$$g = (-6.04\varphi + 0.4705)T + 1722.3\varphi - 134.63 \quad (29)$$

$$\beta = 0.0017 * (100 * \varphi)^{(-0.0841)} \quad (30)$$

It is believed that the thermo-physical characteristics of pure water depend on temperature. The consequent model has been utilized to forecast the thermo-physical characteristics of water [43]

$$\rho = 2446 - 20.674T + 0.11576T^2 - 3.12895 * 10^{-4}T^3 + 4.0505 * 10^{-7}T^4 - 2.0546 * 10^{-10}T^5 \quad (31)$$

$$\mu = 2.414 * 10^{-5} * 10^{\left(\frac{247.8}{T-140}\right)} \quad (32)$$

$$k = -1.13 + 9.71 * 10^{-3}T - 1.31 * 10^{-5}T^2 \quad (33)$$

Mathematical Modeling, Grid-Independent Test, and Validations of Methodology

A 3-D flow domain has been generated using design modular in ANSYS-Fluent as per the physical dimension given in the work of Seyyed et al. [27]. Utilizing the finite volume approach governing equations at specified boundary conditions are resolved. We considered the non-uniform structured grid for the analysis, as depicted in Figure 3. Due to the significant temperature and velocity gradients, the grid points are grouped close to the wall. The approach implemented for solving the problem is the SIMPLE technique. The discretization scheme used for momentum, energy, and pressure is second-order upwind, second-order

Table 2. Properties of nanoparticle and porous media

Particle	Diameter (mm)	C _p (J/(kg.K))	k(W/mK)	ρ(kg/m ³)
Fe ₃ O ₄	0.00002	640	7	4950
Bronze	0.1	343	26	8666

upwind, and presto, respectively. The LSCB (least squares cell-based) method is used for the gradient. The convergence criterion for the momentum and energy thresholds are chosen at 10^{-6} and 10^{-9} , respectively.

The result of numerical analysis depends significantly upon the type of meshes and the number of elements therein. Therefore, it must adopt a typical mesh structure and a certain number of elements beyond which numerical simulation results will not vary appreciably. At different grid numbers, the heat sink's bottom wall temperature was monitored in the axial direction to verify the calculation's correctness and grid independence. Figure 4 summarises the findings, from which we infer that there is a very small difference in the outcomes of simulations with varying

numbers of elements. As a result, around 8 to 9 lac elements were employed throughout all simulations.

To verify the numerical approach, the present results have been compared with the experimental result [27] for a heat sink considering identical geometry, coolant, dimensions, and boundary conditions. Figure 5 compares the present heat transfer coefficient and thermal resistance results to those of Sayyed et al. [27]. The maximal divergence from the numerical findings is 5%, which validates the present finding.

Figure 6 compares the computational and theoretical approaches for calculating the temperature rise of coolant across the channel inlet and outlet. The theoretical predictions are based on the energy balance equation.

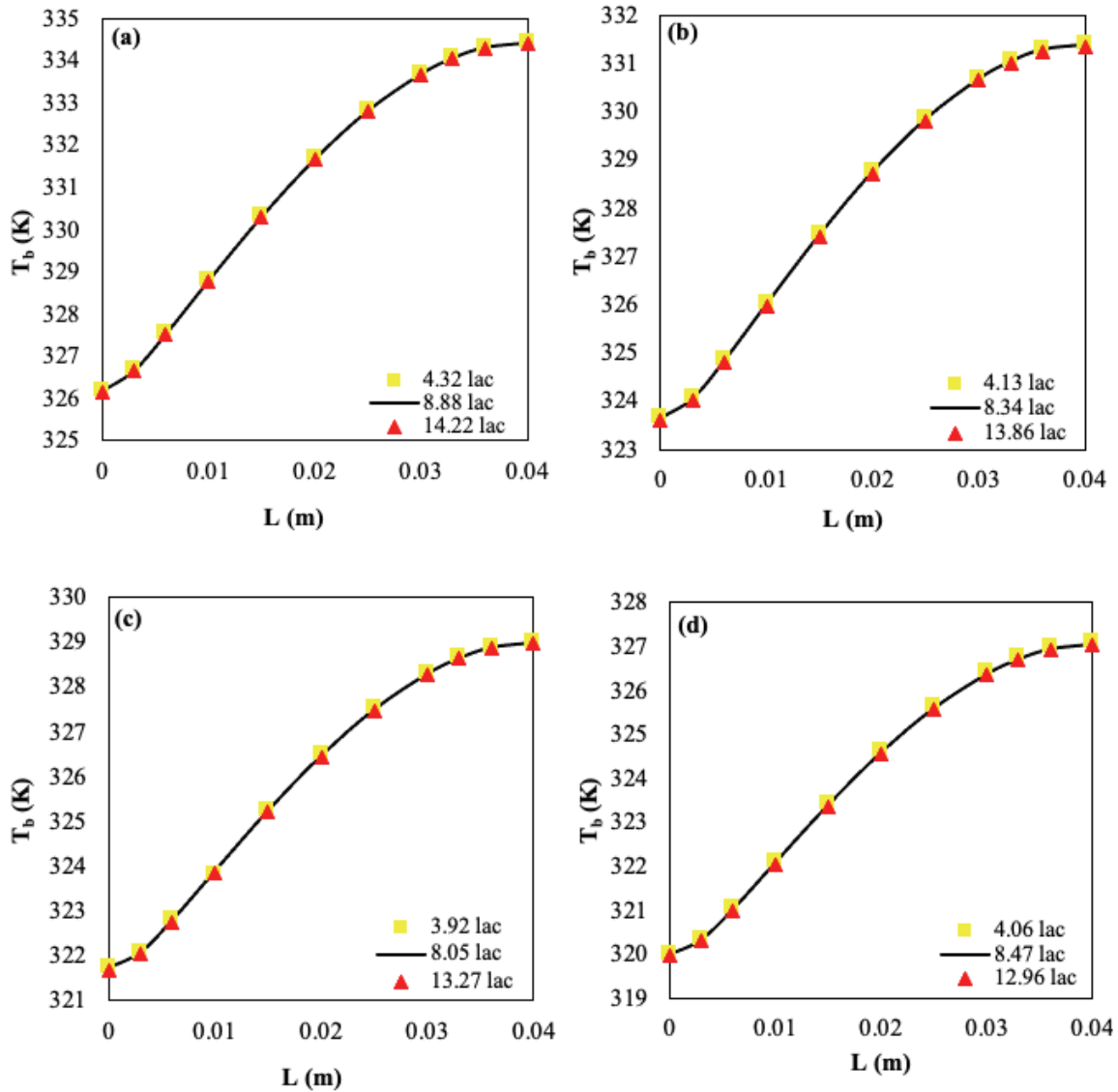


Figure 4. Grid independency test at various channel counts (a) $n=05$ (b) $n=06$ (c) $n=07$ (d) $n=08$ respectively.

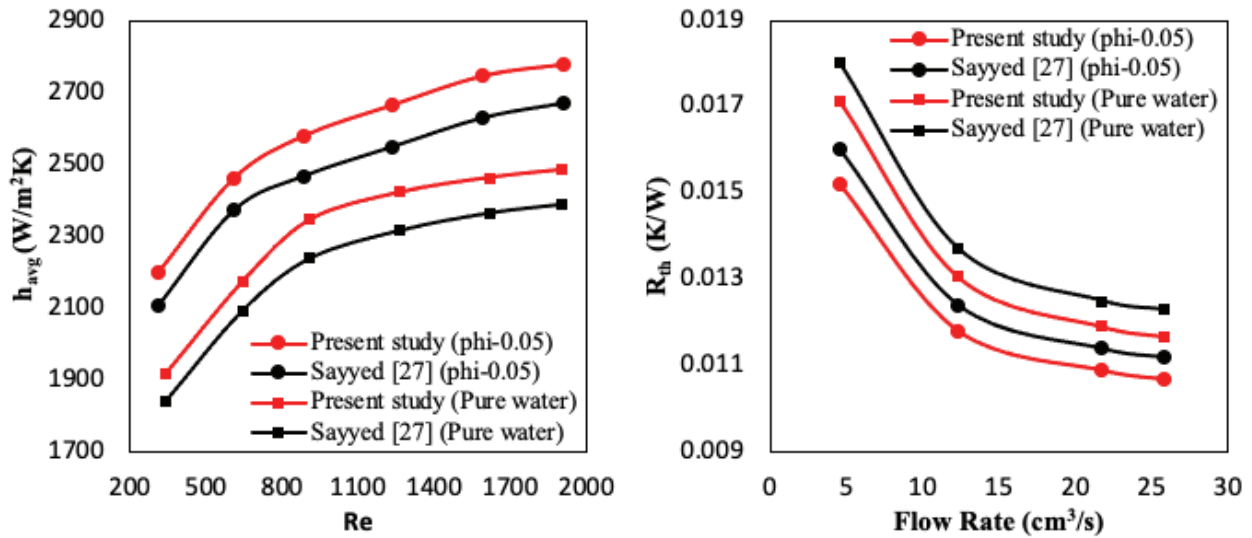


Figure 5. Comparison between the present and Sayyed et al. [27] study.

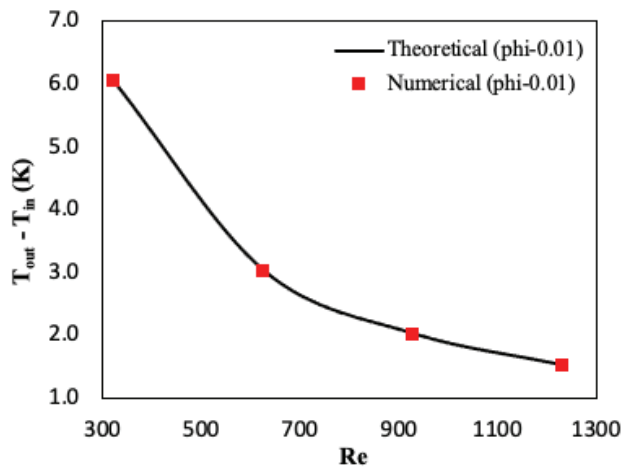


Figure 6. Comparison of numerical data and theoretical energy balance.

$$\rho_f Q C_{p,f} (T_{out} - T_{in}) = q = \dot{q}'' \times A_b \quad (34)$$

The strong alignment of the two demonstrates the reliability of computational approaches.

RESULTS AND DISCUSSION

Heat Transfer Results

In the present study, the impact of heat transfer augmentation techniques on the minichannel heat sink has been investigated numerically. The influence of variations in volume flow rate, nanofluid concentration, and the porosity level of channels on the hydrothermal performance have been studied. To explore the rate of heat

transfer, we determined the coefficient of average heat transfer of the channel. The Variations in the coefficient of heat transfer for five channel counts with volume flow rate and nanofluid concentration are examined for both non-porous and porous channels at various porosity levels, and results are summarized in Figures 7 and 8, respectively. Figure 7(a) depicts that the flow rate and nanoparticle concentration have a direct relationship with the coefficient of heat transfer. At the higher flow rate, the fluid experiences less temperature rise while passing over the heated surface due to a shorter period, and the difference in temperature between the heated surface and fluid is going to rise, causing a higher heat transfer rate. The incorporation of nanoparticles improves the hydrothermal properties of the base fluid, and hence the coefficient of heat transfer is enhanced with a rise in nanoparticle concentration. Figure 7(b) shows that introducing porous media into the flow domain significantly amplifies the heat transmission rate. A porous medium is a solid matrix that is characterized by the presence of void spaces present inside its volume. Because of the solid matrix, a very enormous surface area for heat transfer has been obtained, leading to enhanced heat transmission. Porosity is specified as a ratio of the volume of the void to the entire volume of the channel. If the porosity increases, the void's volume is increased; hence the wetted area of the solid matrix is decreased, which leads to a drop-in heat transfer rate, as we spotted in Figure 8.

Furthermore, we investigate the impact of variation in channel counts of the heat sink on the heat transfer coefficient while keeping the total flow area constant. The hydraulic diameter is inversely proportional to the number of channels at a constant total flow area. An increment in the channel counts of the heat sink will raise the overall surface area, hence the heat transfer will be enhanced.

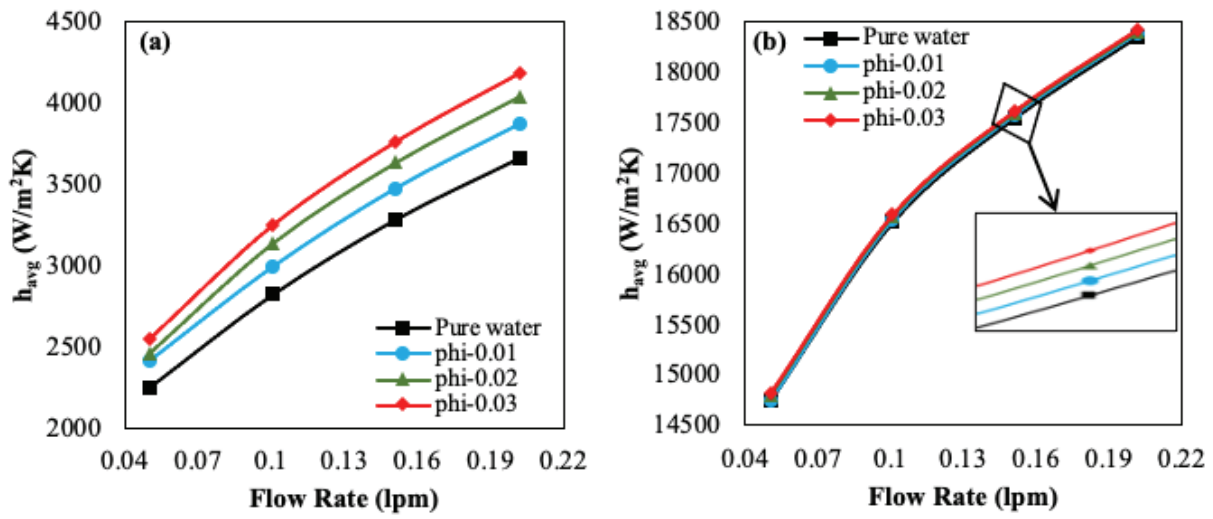


Figure 7. Variation of the average heat transfer coefficient with flow rate for $n=05$ (a) non-porous channel (b) porous channel at $\epsilon=0.75$.

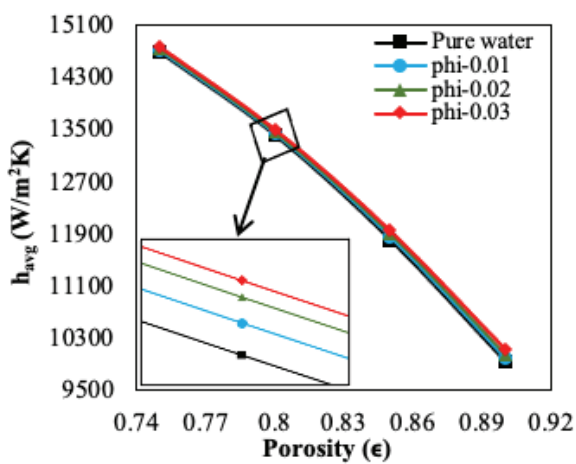


Figure 8. Variation of the average heat transfer coefficient with porosity for $n=05$ at $Q=0.05046$ lpm.

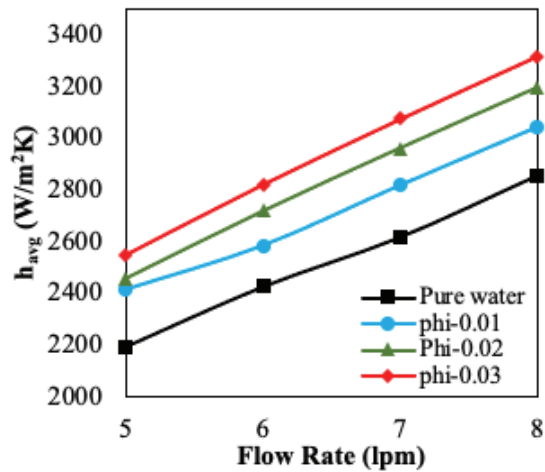


Figure 9. Variation of the average heat transfer coefficient with channel counts (non-porous) at $Q=0.05046$ lpm.

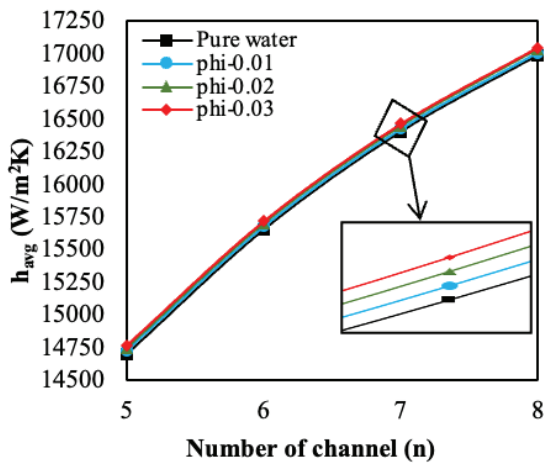


Figure 10. Variation of the average heat transfer coefficient with channel counts (Porous) at $Q=0.05046$ lpm, $\epsilon=0.75$.

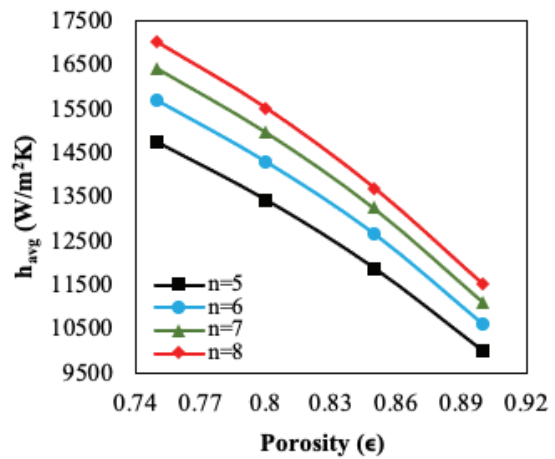


Figure 11. Variation of the average heat transfer coefficient with porosity at $Q=0.05046$ lpm, $\phi=0.01$.

Figures 9 and 10 show that the heat transfer coefficient is increased by increasing the number of channels of the heat sink for both the non-porous and porous types of the flow domain. Figure 11 shows that the heat transfer coefficient is decreased by increasing porosity for all channel counts.

Thermal resistance

Thermal resistance is a crucial evaluation parameter for the heat sink's performance. Hence, for both clear and permeable channels, the thermal resistance variations with volume flow rate and nanofluid concentrations have been determined. Figure 12 shows that the thermal resistance has an inverse relationship with the

volume flow rate and nanofluid concentration. In the presence of a porous media, thermal resistance is much reduced due to the diminished capability of hindering heat dissipation.

From Figure 13, Thermal resistance depends on porosity level; increasing the porosity of the channel leads to enhancing the thermal resistance of the heat sink. Variation in thermal resistance with the channel count is depicted in Figure 14 for non-porous channels and Figures 15 and 16 for the porous channel, respectively. According to these results, increasing the channel count of the heat sink reduced thermal resistance for both non-porous and porous flow domains.

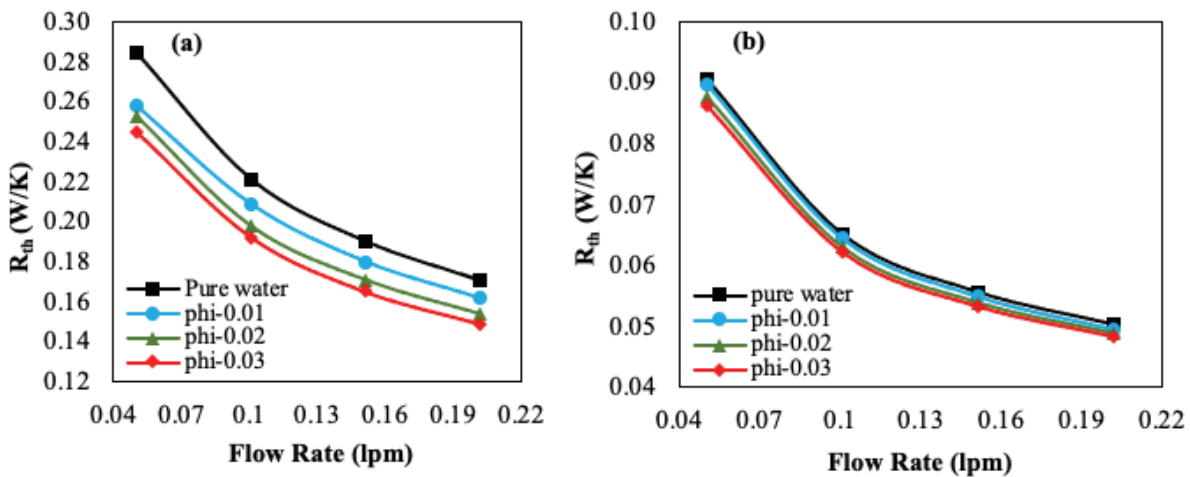


Figure 12. Variation of the thermal resistance with flow rate for $n=05$ (a) clear channel (b) porous channel at $\epsilon=0.75$.

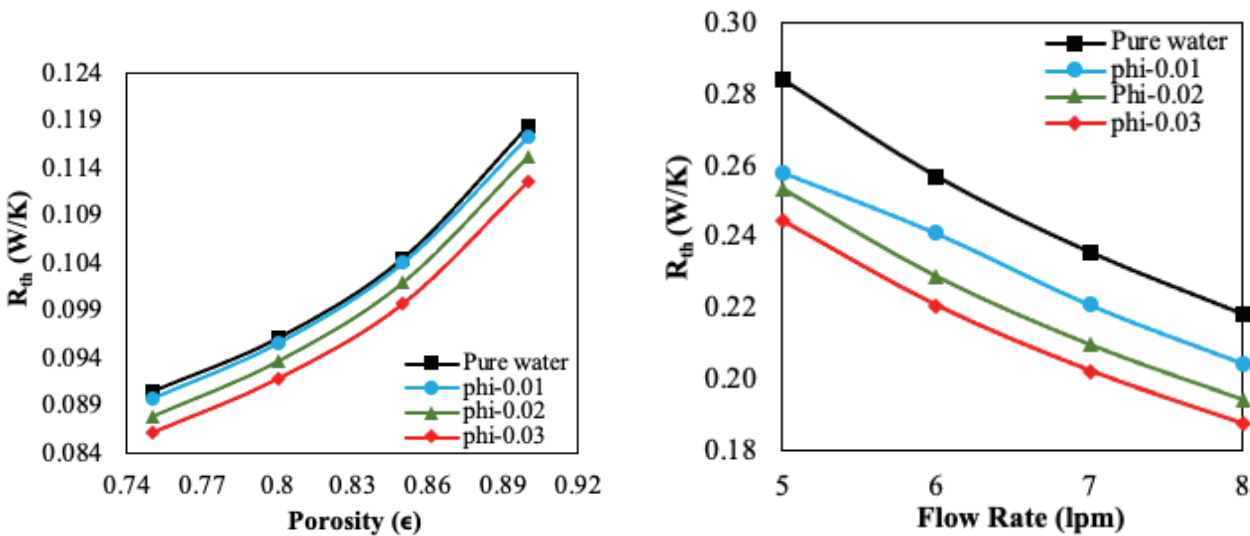


Figure 13. Variation of the thermal resistance with porosity for $n=05$ at $Q=0.05046$ lpm.

Figure 14. Variation of the thermal resistance with channel counts (non-porous) at $Q=0.05046$ lpm.

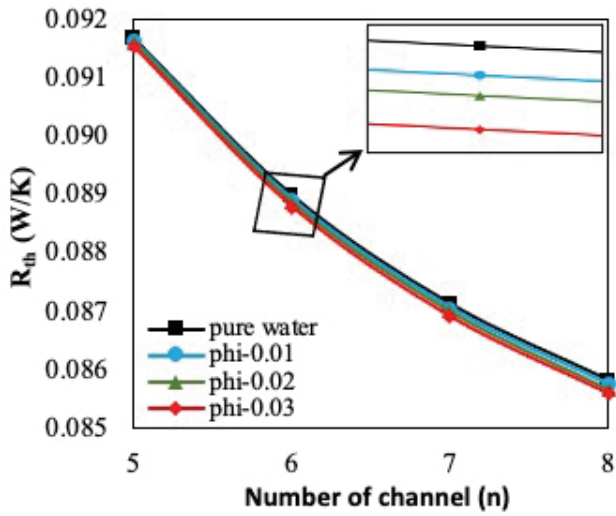


Figure 15. Variation of the thermal resistance with channel counts (Porous) at $Q=0.05046$ lpm, $\epsilon = 0.75$.

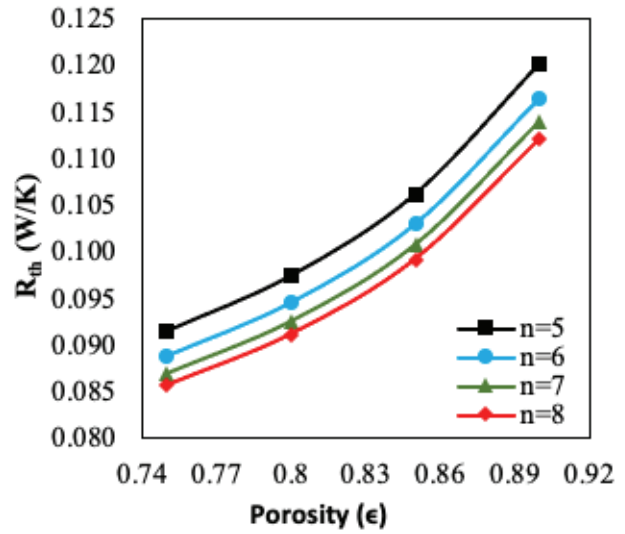


Figure 16. Variation of the thermal resistance with porosity at $Q=0.05046$ lpm, $\phi=0.01$.

Hydrodynamic Results

Pressure drop is another critical criterion for heat sink performance. The pressure drop into the channel is directly consistent with the volume flow rate and the nanoparticle concentrations. Figure 17 illustrates that increasing the mass flow rate and nanofluid concentration raised the pressure drop in both clear and permeable channels. Since the pressure drop across the channel in internal flow is directly correlated with both flow rate and viscosity (eq. 10), hence raising the flow rate increases the pressure drop, and incorporating nanofluid further increases fluid viscosity, which raises the pressure drop once again. In a permeable channel,

frictional loss is increased due to the porous solid matrix which enhances the pressure drop across the channel. As illustrated in Figure 18, higher porosity levels of the porous channel have lowered the pressure drop due to enhanced permeability and less area of contact between the fluid and solid matrix.

Variation in pressure drop with the number of channels is depicted in Figure 19 for the non-porous channels and Figures 20 and 21 for the porous channel, respectively. Pressure drop in any channel is conversely proportional to the fourth power to the diameter of the channel hence at higher channel counts pressure drop is high.

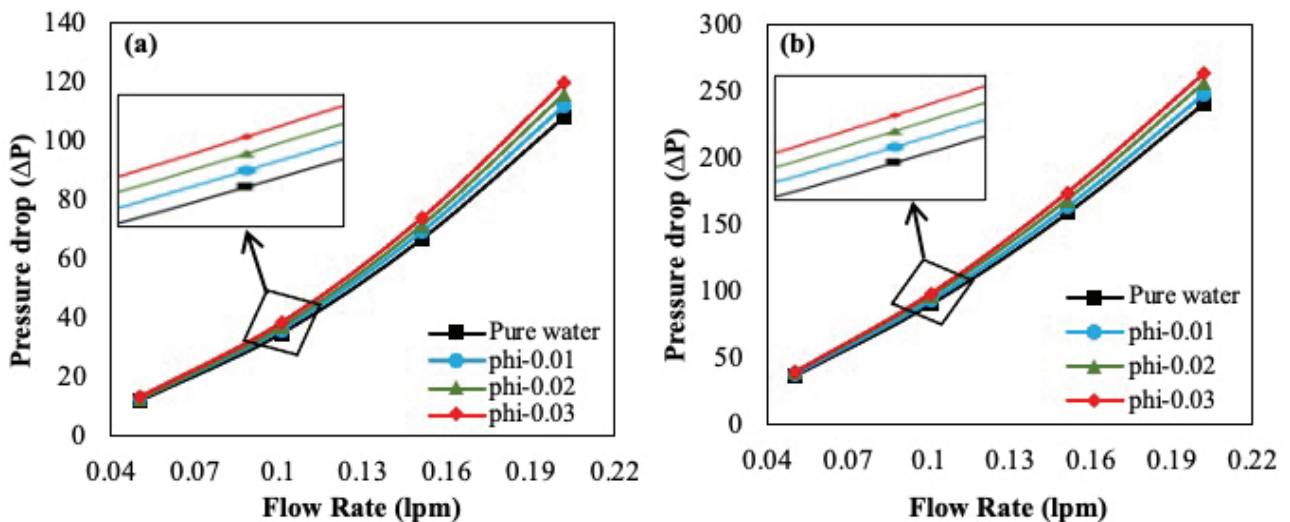


Figure 17. Variation of the pressure drop with flow rate for $n=05$ (a) clear channel (b) porous channel at $\epsilon=0.75$.

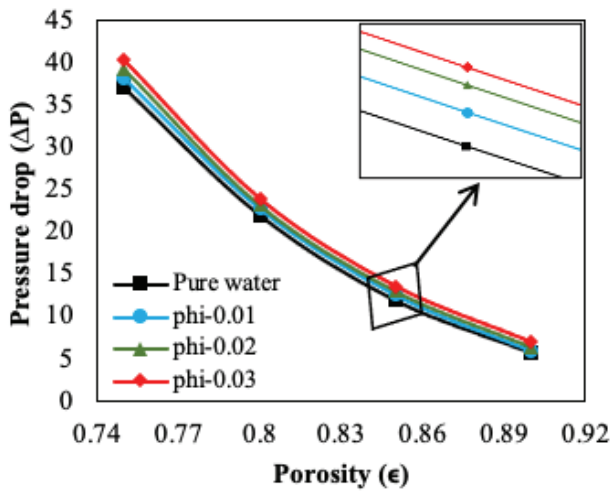


Figure 18. Variation of the pressure drop with porosity for $n=05$ at $Q=0.05046$ lpm.

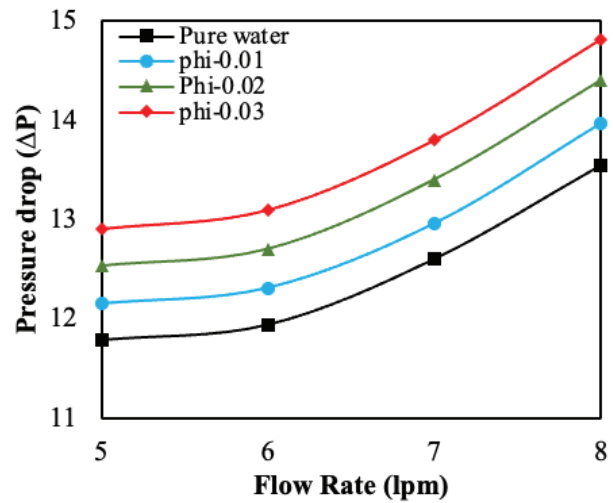


Figure 19. Variation of the pressure drop with channel counts (non-porous) at $Q=0.05046$ lpm.

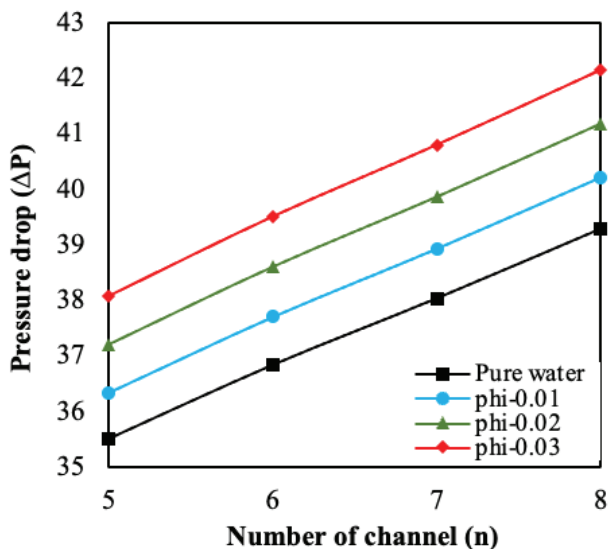


Figure 20. Variation of the pressure drop with channel counts (Porous) at $Q=0.05046$ lpm, $\epsilon=0.75$.

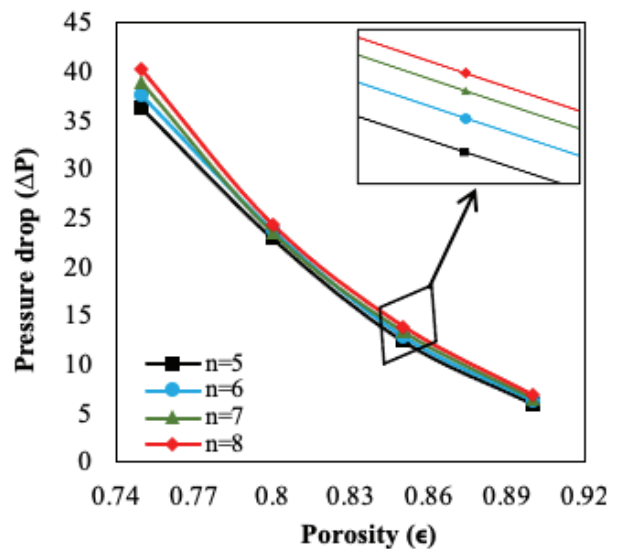


Figure 21. Variation of the pressure drop with porosity at $Q=0.05046$ lpm, $\phi=0.01$.

Evaluation of Hydrothermal Performance

Two factors are primarily responsible for evaluating the performance of the heat sink: coefficient of heat transfer and pressure loss. These characteristics will be imitated by heat transfer efficiency and FOM.

Heat transfer efficiency

The consequences of employing nanofluid and porous media on heat transfer efficiency are explored by comparing the coefficient of average heat transfer relative to the corresponding results of pure water flow through the non-porous channel. Figure 22 depicts how the heat transfer efficiency

of porous and non-porous channels is affected by volume flow rate and nanofluid concentrations.

From Figure 22, It is clear that raising the volume flow rate significantly reduces the heat transfer efficiency of permeable channels compared to clear channels. However, on the other hand, raising the nanofluid concentration prominently improves the heat transfer efficiency for non-porous channels but not remarkably in porous channels. From Figure 23, it was concluded that the porous channels efficiency will decrease steeply by increasing the porosity of the channel. Hence, it is concluded that the heat transfer efficiency is more appreciable for porous heat sinks with lower porosity. By considering all input parameters of the

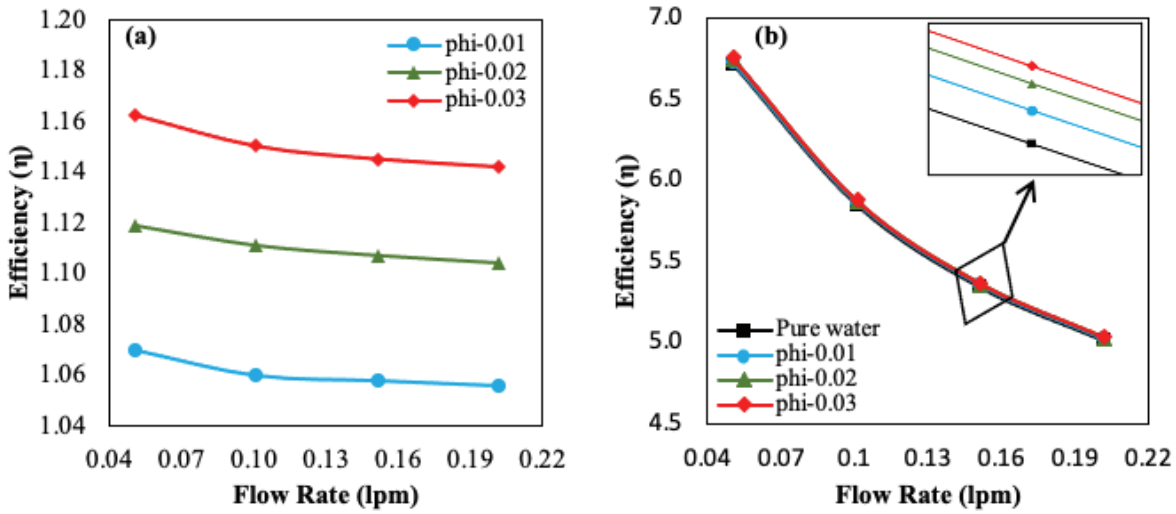


Figure 22. Variation of the heat transfer efficiency with flow rate for n=05 (a) clear channel (b) porous channel at $\epsilon=0.75$.

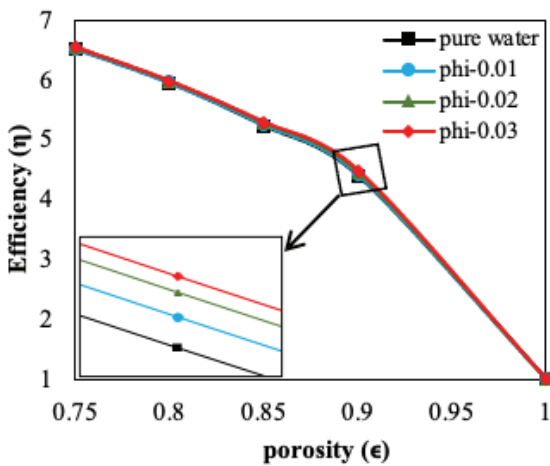


Figure 23. Variation of the heat transfer efficiency with porosity for n=05 at $Q=0.05046$ lpm.

current study; we conclude that the maximum heat transfer efficiency for n=05 is obtained at $Q=0.05046$ lpm, phi-0.03, $\epsilon=0.75$.

Figure 24, it was found that heat transfer efficiency increases from n=5 to n=6 and decreases from n=6 to n=8 for both clear and porous channels despite that it is more prominent with porous media. Hence from the current considerable scenario, we have concluded that n=6 channel count is very efficient in terms of heat transfer.

Table 3 shows the maximum augmentation in heat transfer with channel counts that incorporate either nanofluid or nanofluid combined with porous media. Table 4 shows the maximum augmentation in heat transfer with channel count as compared to the reference study (n=5).

From this study, we found that increasing the channel count is directly associated with the heat transfer rate for both clear and porous heat sinks. However, the optimum

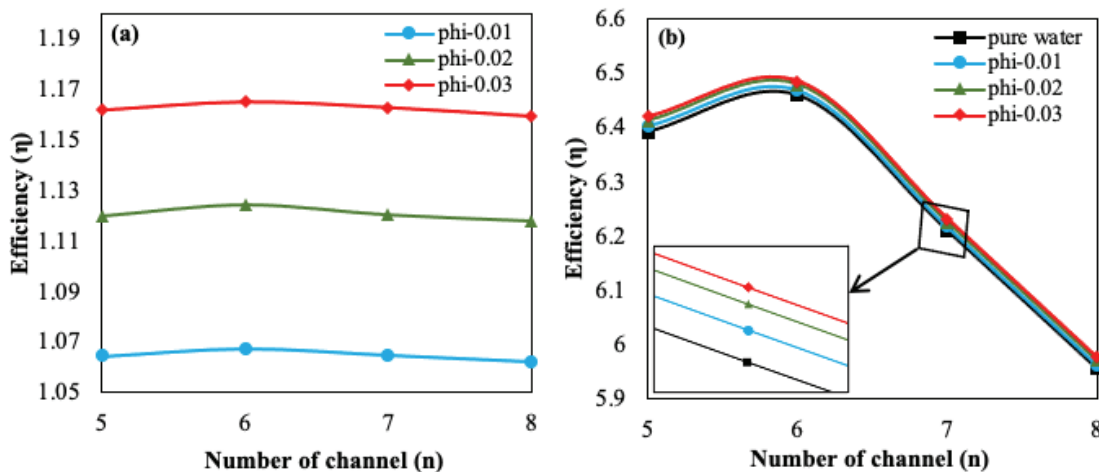


Figure 24. Variation of the heat transfer efficiency with channel counts for (a) $Q=0.05046$ lpm, (b) $Q=0.05046$ lpm, $\epsilon=0.75$.

Table 3. Maximum augmentation in heat transfer

Number of channel(n)	Nanofluid	Nanofluid and porous media
05	12.95 %	548.51%
06	16.33%	554.53%
07	16.16%	523.29%
08	16.00%	497.71%

Table 4. Maximum augmentation in heat transfer compared with the reference study (n=05)

Channel type	n=06	n=07	n=08
Nonporous channel	10.64%	20.56%	30.08%
Porous channel	6.44%	11.51%	15.46%

performance of the present study in terms of heat transfer is attained at the 06-channel count due to the maximum heat transfer efficiency.

Figures of merit (FOM)

The effectiveness of improving the channel's heat transfer ability is again analyzed concerning the figure of merit (FOM). The FOM provides a thorough evaluation of a heat sink's performance. Enhancing the heat transfer coefficient at the expense of the pumping power cost is the foundation of FOM.

Figure 25 depicts the impact of flow rate and nanofluid volume fraction on FOM for both clear and porous channels. The results reveal that for the clear channel, raising the volume flow rate reduces the FOM whereas increases by increasing the nanofluid concentration. However, in a porous channel, FOM decreases by increasing both volume

flow rate and nanofluid concentration. Figure 26 depicts that the FOM is increased with the increased porosity level of the channel since the pumping power is reduced more relative to the augmentation of the heat transfer. Hence, it is concluded that the FOM is more appreciable for porous heat sinks with higher porosity.

Figure 27 shows the variation in FOM for different channel counts. It was found that FOM increased from n=05 to n=06 and decreased from n=06 to n=08 for both clear and porous channels despite that it is more prominent with porous media. Hence from the current considerable scenario, we have concluded that n=6 channel count is very efficient in terms of FOM.

Suppose cooling of the channel is the primary objective then low volume flow rate, high volume fraction, and low porosity are suggested. Because, if we consider FOM and

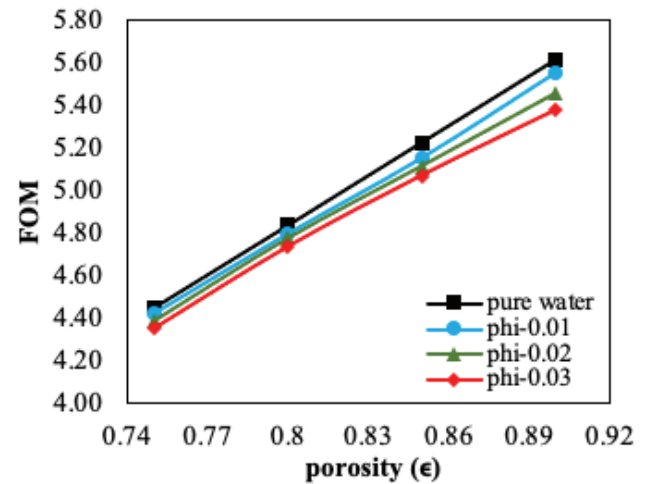


Figure 26. variation of the FOM with porosity for n=05 at Q=0.05046 lpm.

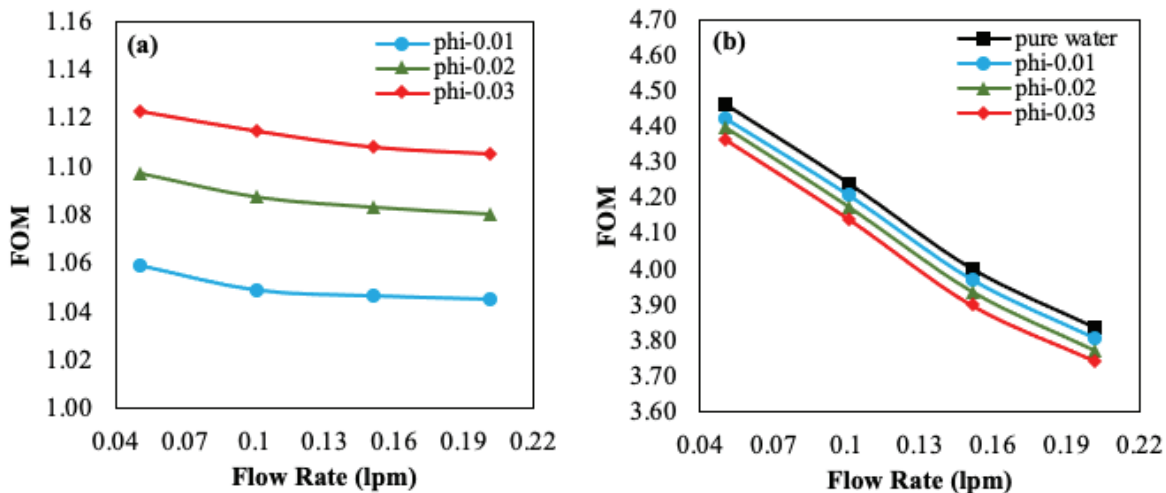


Figure 25. Variation of the FOM with flow rate for n=05 (a) clear channel (b) porous channel at $\epsilon=0.75$.

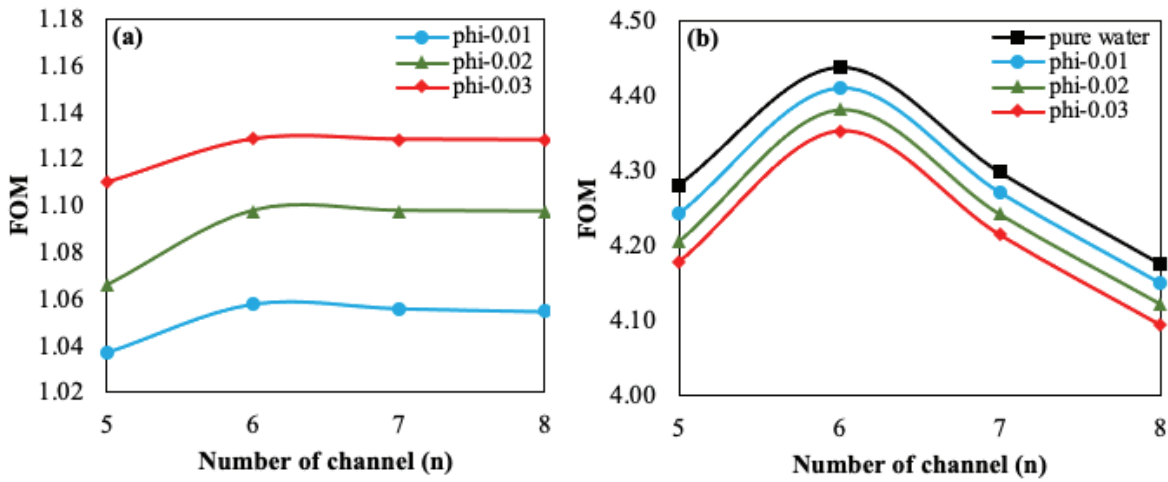


Figure 27. Variation of the FOM with channel counts for (a) $Q=0.05046$ lpm, (b) $Q=0.05046$ lpm, $\epsilon=0.75$.

heat transfer efficiency simultaneously, we observe that the rate of heat transfer dominates over pumping power at low porosity. During the reduction in porosity from $\epsilon=0.9$ to $\epsilon=0.75$, we get maximum enhancement in heat transfer efficiency for the $n=06$ channel is 58.42%. However, the reduction in FOM is 21.4% which is acceptable in terms of cooling.

CONCLUSION

The variations in mass flow rate, nanofluid concentration, and the channel count on the convective heat transfer rate and pressure drop of a circular non-porous, and porous minichannel heat sink with various porosity levels have been investigated numerically. The following outcomes were attained.

- When comparing permeable channels to clear channels, the heat transfer efficiency has been significantly reduced by raising the volume flow rate. However, increasing the nanofluid concentration has improved the heat transfer efficiency in non-porous channels more considerably than in permeable channels.
- When comparing permeable channels to clear channels, the FOM has been significantly reduced by raising the volume flow rate. However, raising the nanofluid concentration has enhanced FOM in non-porous channels while lowering the FOM marginally in porous channels.
- In a permeable channel, increasing the porosity has significantly decreased the heat transfer efficiency while increasing the FOM substantially. During the reduction in porosity from $\epsilon=0.9$ to $\epsilon=0.75$, we get maximum enhancement in heat transfer efficiency at $n=06$ channel is 58.42%. However, the reduction in FOM is 21.4% which recommends that the low porosity level channels provide very significant hydrothermal performances.
- From both heat transfer efficiency and FOM point of view, increasing the channel count in porous MCHS is

relatively more pronounced than in non-porous MCHS. Both heat transfer efficiency and FOM have increased from $n=5$ to $n=6$ while decreasing from $n=6$ to $n=8$ channel count for all volume flow rates and nanofluid volume fractions of porous and non-porous channels. Hence, we have concluded that the $n=6$ channel count provides the best hydrothermal performance.

- The maximum augmentation in heat transfer compared with pure water flow in a non-porous channel is achieved at six channel count with an increment of 16.6% due to the insertion of nanofluid and 554.53% by the simultaneous incorporation of porous media and nanofluid.
- Achieving optimum performance of the heat sink by considering both FOM and heat transfer efficiency simultaneously, the rigorous performance is achieved at six channel count with a lower volume flow rate, a higher volume fraction of nanofluid, and a lower porosity level.

NOMENCLATURE

3-D	Three dimensional
A_b	Bottom wall area for unit cell
A_t	Bottom wall area of the heat sink
A_c	The cross-sectional area of the channel
A_h	Convective area of heat transfer
C_p	Specific heat (KJ/Kg-k)
CFD	Computational fluid dynamics
D_h	Hydraulic diameter (m)
FF	Frictional factor ($\Delta PD_h/2L\rho V^2$)
FOM	Figures of merit
h_{av}	Average heat transfer coefficient ($W/m^2 K$)
k	Thermal conductivity ($W/m K$)
K_p	Permeability of porous media (m^2)
lpm	Litre per minute
n	Number of channels

Nu	Nusselt number (hD_h/k)
ΔP	Pressure drop (ΔP)
PP	Pumping power ($\Delta P \cdot Q$)
q	Total heating power (W)
$q^{''}$	Heat flux (W/m^2)
Q	Volume flow rate for unit channel (lpm)
Q_t	Total volume flow rate (lpm)
R_{th}	Thermal resistance (K/W)
V	Velocity (m/s)
T	Temperature (K)

Greek symbols

β	Fraction of liquid volume
μ	Dynamic viscosity ($N \cdot s/m^2$)
ϕ	Volume fraction
ϵ	porosity
ρ	Density (kg/m^3)
η	Heat transfer efficiency
Γ	The interface of solid and liquid

Subscripts

av	Average
b	Bottom
ba	Interface surface
bu	Bulk mean
c	channel
cf	Non-porous channel with water as a coolant
eff	Effective
f	Fluid
fl	Final
i	Initial
in	Inlet
max	maximum
nf	Nanofluid
np	Nanoparticle
out	Outlet
s	Solid
w	wall

AUTHORSHIP CONTRIBUTIONS

Authors equally contributed to this work.

DATA AVAILABILITY STATEMENT

The authors confirm that the data that supports the findings of this study are available within the article. Raw data that support the finding of this study are available from the corresponding author, upon reasonable request.

CONFLICT OF INTEREST

The authors declared no potential conflicts of interest with respect to the research, authorship, and/or publication of this article.

ETHICS

There are no ethical issues with the publication of this manuscript.

REFERENCES

- [1] Tuckerman DB, Pease RFW. High-Performance Heat Sinking for VLSI. *IEEE Electr Dev Lett* 1981;2:126–129. [\[CrossRef\]](#)
- [2] Morini GL. Single-phase convective heat transfer in microchannels: A review of experimental results. *Int J Therm Sci* 2004;43:631–651. [\[CrossRef\]](#)
- [3] Mustafizur Rahman M. Measurements of heat transfer in microchannel heat sinks. *Int Commun Heat Mass Transf* 2000;27:495–506. [\[CrossRef\]](#)
- [4] Qu W, Mudawar I. Analysis of three-dimensional heat transfer in micro-channel heat sinks. *Int J Heat Mass Transf* 2002;45:3973–3985. [\[CrossRef\]](#)
- [5] Ghasemi SE, Ranjbar AA, Hosseini MJ. Numerical study on effect of CuO-water nanofluid on cooling performance of two different cross-sectional heat sinks. *Adv Powder Technol* 2017;28:1495–1504. [\[CrossRef\]](#)
- [6] Knight RW, Goodling JS, Hall DJ. Optimal thermal design of forced convection heat sinks-analytical. *J Elect Packaging* 1991;113:313–321. [\[CrossRef\]](#)
- [7] Knight RW, Hall DJ, Goodling JS, Jaeger RC. Heat sink optimization with application to microchannels. 1992;15:832–842. [\[CrossRef\]](#)
- [8] Mohammed HA, Gunnasegaran P, Shuaib NH. The impact of various nanofluid types on triangular microchannels heat sink cooling performance. *Int Commun Heat Mass Transf* 2011;38:767–773. [\[CrossRef\]](#)
- [9] Khodabandeh E, Abbassi A. Performance optimization of water-Al₂O₃ nanofluid flow and heat transfer in trapezoidal cooling microchannel using structural theory and two-phase Eulerian-Lagrangian approach. *Powder Technol* 2018;323:103–114. [\[CrossRef\]](#)
- [10] Hung TC, Yan WM. Effects of tapered-channel design on thermal performance of microchannel heat sink. *Int Commun Heat Mass Transf* 2012;39:1342–1347. [\[CrossRef\]](#)
- [11] Dehghan M, Daneshipour M, Valipour MS, Rafee R, Saedodin S. Enhancing heat transfer in micro-channel heat sinks using converging flow passages. *Energy Convers Manag* 2015;92:244–250. [\[CrossRef\]](#)
- [12] Chai L, Xia GD, Wang HS. Numerical study of laminar flow and heat transfer in microchannel heat sink with offset ribs on sidewalls. *Appl Therm Eng* 2016;92:32–41. [\[CrossRef\]](#)
- [13] Yildizeli A, Cadirci S. Multi-objective optimization of a micro-channel heat sink through genetic algorithm. *Int J Heat Mass Transf* 2020;146:118847. [\[CrossRef\]](#)

- [14] Kose HA, Yildizeli A, Cadirci S. Parametric study and optimization of microchannel heat sinks with various shapes. *Appl Therm Eng* 2022;211:118368. [\[CrossRef\]](#)
- [15] Pak BC, Cho YI. Hydrodynamic and heat transfer study of dispersed fluids with submicron metallic oxide particles. *Exp Heat Transf* 1998;11:151–170. [\[CrossRef\]](#)
- [16] Hosseini SR, Sheikholeslami M, Ghasemian M, Ganji DD. Nanofluid heat transfer analysis in a microchannel heat sink under the effect of magnetic field by means of KKL model. *Powder Technol* 2018;324:36–47. [\[CrossRef\]](#)
- [17] Xuan Y, Li Q. Investigation on convective heat transfer and flow features of nanofluids. *J Heat Transf* 2003;125:151–155. [\[CrossRef\]](#)
- [18] Alawi OA, Sidik NAC, Xian HW, Kean TH, Kazi SN. Thermal conductivity and viscosity models of metallic oxides nanofluids. *Int J Heat Mass Transf* 2018;116:1314–1325. [\[CrossRef\]](#)
- [19] Koo J, Kleinstreuer C. Laminar nanofluid flow in microheat-sinks. *Int J Heat Mass Transf* 2005;48:2652–2661. [\[CrossRef\]](#)
- [20] Chein R, Huang G. Analysis of microchannel heat sink performance using nanofluids. *Appl Therm Eng* 2005;25:3104–3114. [\[CrossRef\]](#)
- [21] Ho CJ, Chen WC. An experimental study on thermal performance of Al₂O₃/water nanofluid in a minichannel heat sink. *Appl Therm Eng* 2013;50:516–522. [\[CrossRef\]](#)
- [22] Soheli MR, Saidur R, Khaleduzzaman SS, Ibrahim TA. Cooling performance investigation of electronics cooling system using Al₂O₃-H₂O nanofluid. *Int Commun Heat Mass Transf* 2015;65:89–93. [\[CrossRef\]](#)
- [23] Hung TC, Yan WM, Wang XD, Chang CY. Heat transfer enhancement in microchannel heat sinks using nanofluids. *Int J Heat Mass Transf* 2012;55:2559–2570. [\[CrossRef\]](#)
- [24] Bahiraei M, Heshmatian S. Optimizing energy efficiency of a specific liquid block operated with nanofluids for utilization in electronics cooling: A decision-making based approach. *Energy Convers Manag* 2017;154:180–190. [\[CrossRef\]](#)
- [25] Bhattacharya P, Samanta AN, Chakraborty S. Numerical study of conjugate heat transfer in rectangular microchannel heat sink with Al₂O₃/H₂O nanofluid. *Heat Mass Transf* 2009;45:1323–1333. [\[CrossRef\]](#)
- [26] Lelea D. The performance evaluation of Al₂O₃/water nanofluid flow and heat transfer in microchannel heat sink. *Int J Heat Mass Transf* 2011;54:3891–3899. [\[CrossRef\]](#)
- [27] Sayeed AF, Hosseini Hashemi SM, Zirakzadeh H, Ashjaee M. Experimental and numerical investigation of heat transfer in a miniature heat sink utilizing silica nanofluid. *Superlattices Microstruct* 2012;51:247–264. [\[CrossRef\]](#)
- [28] Soheli MR, Khaleduzzaman SS, Saidur R, Hepbasli A, Sabri MFM, Mahbubul IM. An experimental investigation of heat transfer enhancement of a minichannel heat sink using Al₂O₃-H₂O nanofluid. *Int J Heat Mass Transf* 2014;74:164–172. [\[CrossRef\]](#)
- [29] Kumar V, Sarkar J. Experimental hydrothermal behavior of hybrid nanofluid for various particle ratios and comparison with other fluids in minichannel heat sink. *Int Commun Heat Mass Transf* 2020;110:104397. [\[CrossRef\]](#)
- [30] Goud JS, Srilatha P, Varun Kumar RS, Kumar KT, Khan U, Raizah Z, et al. Role of ternary hybrid nanofluid in the thermal distribution of a dovetail fin with the internal generation of heat. *Case Stud Therm Eng* 2022;35:102113. [\[CrossRef\]](#)
- [31] Zahan I, Nasrin R, Khatun S. Thermal performance of ternary-hybrid nanofluids through a convergent-divergent nozzle using distilled water-ethylene glycol mixtures. *Int Commun Heat Mass Transf* 2022;137:106254. [\[CrossRef\]](#)
- [32] Awad A, Ahmed W, Waleed M. Nanotechnology for energy storage. *Emerging Nanotechnol Renewable Energy* 2021:495–516. [\[CrossRef\]](#)
- [33] Awad AT, Muayad MW. Experimental heat transfer study of an enhanced storage medium. *J Energy Storage* 2023;73: 2023.108953. [\[CrossRef\]](#)
- [34] Luo X, Li W, Wang Q, Zeng M. Numerical investigation of a thermal energy storage system based on the serpentine tube reactor. *J Energy Storage* 2022;56:106071. [\[CrossRef\]](#)
- [35] Younis O, Mourad A, Aissa A, Qasem NAA, Abed AM, Akbari OA, et al. Numerical investigation of thermal energy storage system loaded with nano-enhanced phase change material with Koch snowflake fractal cross-section. *J Energy Storage* 2022;56:106016. [\[CrossRef\]](#)
- [36] Jahanbakhshi A, Nadooshan AA, Bayareh M. Cooling of a lithium-ion battery using microchannel heatsink with wavy microtubes in the presence of nanofluid. *J Energy Storage* 2022;49:104128. [\[CrossRef\]](#)
- [37] Khaled ARA, Siddique M, Abdulhafiz NI, Boukhary AY. Recent advances in heat transfer enhancements: A review report. *Int J Chem Eng* 2010:106461. [\[CrossRef\]](#)
- [38] Koh JCY, Colony R. Analysis of cooling effectiveness for porous material in a coolant passage. *J Heat Transf* 1974;96:324–330. [\[CrossRef\]](#)
- [39] Hunt ML, Tien CL. Effects of thermal dispersion on forced convection in fibrous media. *Int J Heat Mass Transf* 1988;31:301–309. [\[CrossRef\]](#)
- [40] Zehforoosh A, Hossainpour S. Numerical investigation of pressure drop reduction without surrendering heat transfer enhancement in partially porous channel. *Int J Therm Sci* 2010;49:1649–1662. [\[CrossRef\]](#)

- [41] Wang B, Hong Y, Wang L, Fang X, Wang P, Xu Z. Development and numerical investigation of novel gradient-porous heat sinks. *Energy Convers Manag* 2015;106:1370–1378. [\[CrossRef\]](#)
- [42] Saravanan V, Umesh CK. Effect of porous medium on thermo-hydraulic performance of micro channel heat sink. 2017;12:599–612.
- [43] Bezaatpour M, Goharkhah M. Three-dimensional simulation of hydrodynamic and heat transfer behavior of magnetite nanofluid flow in circular and rectangular channel heat sinks filled with porous media. *Powder Technol* 2019;344:68–78. [\[CrossRef\]](#)
- [44] Dai H, Chen W, Dong X, Liu Y, Cheng Q. Thermohydraulic performance analysis of graded porous media microchannel with microencapsulated phase change material suspension. *Int J Heat Mass Transf* 2021;176:121459. [\[CrossRef\]](#)
- [45] Pati S, Borah A, Boruah MP, Randive PR. Critical review on local thermal equilibrium and local thermal non-equilibrium approaches for the analysis of forced convective flow through porous media. *Int Commun Heat Mass Transf* 2022;132:105889. [\[CrossRef\]](#)
- [46] Alhajaj Z, Bayomy AM, Saghir MZ, Rahman MM. Flow of nanofluid and hybrid fluid in porous channels: Experimental and numerical approach. *Int J Thermofluids* 2020;1–2:100016. [\[CrossRef\]](#)
- [47] Sivasankaran S, Bhuvanewari M. Numerical study on influence of water-based hybrid nanofluid and porous media on heat transfer and pressure loss. *Case Stud Therm Eng* 2022;34:102022. [\[CrossRef\]](#)
- [48] Rashidi S, Ijadi A, Dadashi Z. Potentials of porous materials for temperature control of lithium-ion batteries. *J Energy Storage* 2022;51:104457. [\[CrossRef\]](#)
- [49] Kaabinejadian A, Ahmadi HA, Moghimi M. Investigation of porous media effects on lithium-ion battery thermal management. *J Therm Anal Calorim* 2020;141:1619–1633. [\[CrossRef\]](#)
- [50] Hoseini SS, Seyedkanani A, Najafi G, Sasmito AP, Akbarzadeh A. Multiscale architected porous materials for renewable energy conversion and storage. *Energy Storage Mater* 2023;59:102768. [\[CrossRef\]](#)